CHEMISTRY OF MATERIALS
Article

Chem. Mater. **2010,** *22,* 5209–5215 5209
DOI:10.1021/cm101164r

Nanosize-Controlled Syntheses of Indium Metal Particles and Hollow Indium Oxide Particles via the Sputter Deposition Technique in Ionic Liquids

Toshimasa Suzuki,[†] Ken-ichi Okazaki,[†] Shushi Suzuki,[†] Tamaki Shibayama,[‡] Susumu Kuwabata,[§,⊥] and Tsukasa Torimoto*[,†,⊥]

[†]*Graduate School of Engineering, Nagoya University, Furo-cho, Chikusa-ku, Nagoya 464-8603, Japan,* [‡]*Center for Advanced Research of Energy Conversion Materials, Hokkaido University, Sapporo, Hokkaido 060-8628, Japan,* [§]*Graduate School of Engineering, Osaka University, Suita, Osaka 565-0871, Japan, and* [⊥]*Japan Science and Technology Agency, CREST, Kawaguchi, Saitama 332-0012, Japan*

Received April 26, 2010. Revised Manuscript Received August 3, 2010

Sputter deposition of indium (In) in ionic liquids (ILs) could produce stable In metal nanoparticles whose surface was covered by an amorphous In_2O_3 layer to form In/In_2O_3 core/shell particles. The size of the In core was tunable from ca. 8 to 20 nm by selecting the kind of IL, whereas the shell thickness of In_2O_3 was almost constant at ca. 1.9 nm. Heat treatment of the thus-obtained particles at 523 K in air oxidized In metal of the core, resulting in the formation of spherical hollow particles made of crystalline In_2O_3. The size of the hollow particles was slightly larger than that of the In/In_2O_3 core/shell particles used as a starting material, whereas the void space formed inside hollow particles was smaller than the corresponding In metal cores. These facts indicated that in addition to the predominant outward diffusion of In ions, an inward transport of oxygen ions occurred, and thus an In_2O_3 crystal could be grown on both the inner concave and outer convex surfaces of the oxide shell layer.

1. Introduction

Structure control of metal and semiconductor nanoparticles in nanometer scale has attracted much attention because the physicochemical properties, such as optical properties and catalytic activities, can be varied depending on the size and shape of nanoparticles.[1−6] Recently, ionic liquids (ILs) have been considered to be excellent media for the formation and stabilization of nanoparticles.[7−9] Noble metal nanoparticles were prepared in ILs without addition of stabilizing agents or capping molecules, in contrast to the synthesis in aqueous or conventional organic solvents, which inevitably requires the addition of stabilizing agents. For example, stable noble metal nanoparticles, such as Ir, Rh, and Au, were chemically synthesized in ILs by chemical reduction of the corresponding metal ions or thermal decomposition of organometallic compounds.[10−12] Although many strategies for the preparation of noble metal nanoparticles have been reported, highly reactive metal nanoparticles, such as Zn and In, which have relatively more negative redox potentials, have been difficult to synthesize in the form of nanometer-sized particles because of the instability of particles induced by easy oxidation reaction in air.

Recently, the extremely low vapor pressure of ILs has enabled researchers to treat them under vacuum conditions.[13,14] Endres et al. reported synthesis of Ag nanoparticles in an IL by reduction of Ag ions in the IL with electrons produced by a glow discharge (plasma-electrochemical deposition) under reduced pressure conditions.[15,16] We previously reported a very clean method for synthesizing noble nanoparticles, such as Au, Ag, and Pt, in ILs using a sputter deposition technique without any additives.[17−20] The size of prepared particles varied depending on the kind of IL used.[17]

*Corresponding author. E-mail: torimoto@apchem.nagoya-u.ac.jp. Tel.: +81-52-789-4614. Fax: +81-52-789-5299.

(1) Kamat, P. *J. Phys. Chem. C* **2007**, *111*, 2834.
(2) Muszynski, R.; Seger, B.; Kamat, P. *J. Phys Chem. C* **2008**, *112*, 5263.
(3) Caruso, F.; Spasova, M.; Saigueirino-Maceira, V.; Liz-Marzan, L. *Adv. Mater.* **2001**, *13*, 1090.
(4) Riha, S.; Parkinson, B.; Prieto, A. *J. Am. Chem. Soc.* **2009**, *131*, 12054.
(5) Nakashima, T.; Kobayashi, Y.; Kawai, T. *J. Am. Chem. Soc.* **2009**, *131*, 11302.
(6) Saruyama, M.; Kanehara, M.; Teranishi, T. *J. Am. Chem. Soc.* **2010**, *132*, 3280.
(7) Scheeren, C.; Machado, G.; Dupont, J.; Fichtner, P.; Texeira, S. *Inorg. Chem.* **2003**, *42*, 4738.
(8) Migowski, P.; Machado, G.; Texeira, S.; Alves, M.; Morais, J.; Traverse, A.; Dupont, J. *Phys. Chem. Chem. Phys.* **2007**, *9*, 4814.
(9) Redel, E.; Thomann, R.; Janiak, C. *Chem. Commun.* **2008**, 1789.
(10) Dupont, J.; Fonseca, G.; Umpierre, A.; Fichtner, P.; Teixeira, S. *J. Am. Chem. Soc.* **2002**, *124*, 4228.
(11) Fonseca, G.; Umpierre, A.; Fichtner, P.; Teixeira, S.; Dupont, J. *Chem.—Eur. J.* **2003**, *9*, 3263.
(12) Guo, S.; Shi, F.; Gu, Y.; Yang, J.; Deng, Y. *Chem. Lett.* **2005**, *34*, 830.
(13) Kuwabata, S.; Kongkanand, A.; Oyamatsu, D.; Torimoto, T. *Chem. Lett.* **2006**, *35*, 600.
(14) Smith, E.; Villar Garcia, I.; Briggs, D.; Licence, P. *Chem. Commun.* **2005**, 5633.
(15) El Abedin, S.; Polleth, M.; Meiss, S.; Janek, J.; Endres, F. *Green Chem.* **2007**, *9*, 549.
(16) Meiss, S.; Rohnke, M.; Kienle, L.; El Abedin, S.; Endres, F.; Janek, J. *ChemPhysChem* **2007**, *8*, 50.
(17) Torimoto, T.; Okazaki, K.; Kiyama, T.; Hirahara, K.; Tanaka, N.; Kuwabata, S. *Appl. Phys. Lett.* **2006**, *89*, 243117.
(18) Okazaki, K.; Kiyama, T.; Hirahara, K.; Tanaka, N.; Kuwabata, S.; Torimoto, T. *Chem. Commun.* **2008**, 691.

Published on Web 08/19/2010

This strategy can be applicable to the synthesis of highly reactive metal particles.

Nanoparticles of indium (In) metal have attracted much attention because they are expected to act as nanometer-sized lubricants or novel catalysts for organic syntheses. Particles of In have been useful as a starting material for the preparation of nanostructured In-based materials because indium is a highly reactive metal and the reaction of nanosized In metal with chemical species containing elements of V or VI groups can produce semiconductor nanoparticles such as InP, InAs, and In_2O_3.[21−23] In nanoparticles have been prepared by several synthetic strategies, such as reduction of In^{3+} ions with strong reducing agents,[24] thermal decomposition of organometallic precursors,[25] laser ablation,[26] metal vapor deposition,[27] and dispersion of molten In into paraffin oil.[28] On the other hand, the preparation of nanostructured In_2O_3 is also attractive because their applications are expected in wide research areas, such as gas sensors,[29] solar cells,[30] flat-panel displays,[31] and photocatalysts.[32] One of the attractive strategies for preparation of In_2O_3 nanoparticles has been oxidation of In particles. The shape of the resulting In_2O_3 particles is expected to be reflected by that of the starting In metal nanoparticles, but the details are not reported for nanometer-sized particles.

In this study, we prepared In metal nanoparticles in ILs by the sputter deposition technique. The thus-obtained In particles were used as a starting material to fabricate nanostructured In_2O_3 particles, and heat treatment of ILs containing In metal particles in air enabled the formation of hollow In_2O_3 nanoparticles highly dispersed in ILs.

2. Experimental Section

Ionic Liquids. Four kinds of imidazolium-based ILs with tetrafluoroborate (BF_4) anion, 1-ethyl-3-methylimidazolium tetrafluoroborate (EMI-BF_4), 1-butyl-3-methylimidazolium tetrafluoroborate (BMI-BF_4), 1-allyl-3-methylimidazolium tetrafluoroborate (AMI-BF_4), and 1-allyl-3-ethylimidazolium tetrafluoroborate (AEI-BF_4) were purchased from Kanto Chemical. The ILs were dried for 3 h at 393 K under a vacuum just before use.

Sputter Deposition of Indium Nanoparticles and Their Oxidation in Air. Sputter deposition of indium in ILs was performed using a sputter coater (Sanyu Electron Co., Ltd., SC-701HMCII) with a sputtering current of 10 mA under argon (>99.99%) pressure of 2.0 Pa at room temperature. An ionic liquid (0.60 cm^3) was spread on a glass plate (10 cm^2) that was horizontally set in the sputter coater. The surface of the IL was located at a distance of 20 mm from the indium foil target (99.99% in purity). The sputtering was carried out for 10 min. After the sputter deposition of In, the vacuum chamber was filled with air and the IL solution was them collected from the glass plate. In the case of oxidation of In particles, a 0.10 cm^3 portion of thus-obtained IL solution was put in a test tube, followed by heat treatment in air at various temperatures for 1 h without agitation.

Characterization of Nanoparticles. The size and shape of nanoparticles formed in ILs were observed using a transmission electron microscope (TEM; HITACHI H-7650) operated at an acceleration voltage of 100 kV. High-resolution transmission electron micrographs of nanoparticles were obtained using a JEOL 2010F TEM operated at 200 kV. Samples for TEM measurements were prepared by dropping an IL solution containing nanoparticles onto a copper grid with amorphous carbon overlayers (Oken Shoji, 10−1012), and the excess amount of IL was then washed out by dropping a small amount of acetonitrile, followed by drying under a vacuum. The size distribution of particles in ILs was also obtained by dynamic light scattering operated at 298 K using an Otuka Electronics FDLS-3000.

The crystal structure of particles was investigated by an X-ray powder diffraction (XRD) analysis using a RIGAKU 2100HL with Cu Kα radiation. X-ray photoelectron spectroscopy (XPS) measurements were performed using a JEOL JPS-9000MC with irradiation of Al Kα. Samples for XRD measurements were prepared by isolation of nanoparticles with the addition of a large amount of methanol to the IL solutions. The precipitates were collected by centrifugation, followed by washing with methanol several times and drying under vacuum.

3. Results and Discussion

Characterization of Particles Prepared by In Sputter Deposition in EMI-BF_4. The XRD pattern of the product obtained sputter deposition of indium in EMI-BF_4 is shown in Figure S1 in the Supporting Information. As can be seen from the figure, several peaks were observed and they were assigned to the body-centered tetragonal (bct) crystal structure of In metal.[33] No perceivable peaks assigned to its derivatives, such as In_2O_3, were observed.[34] The crystallite size of thus-obtained In metal was estimated to be 4.8 nm from the full width at half-maximum of the (101) peak by using the Scherrer equation.[35] In contrast, observation of the dynamic light scattering (DLS) showed that the as-deposited particles in ILs had a wide size distribution ranging from 7 to 10 nm (see Figure S2 in the Supporting Information), and the average diameter was determined to 8.1 nm. This value was remarkably different

(19) Suzuki, T.; Okazaki, K.; Kiyama, T.; Kuwabata, S.; Torimoto, T. *Electrochemistry* **2009**, *77*, 638.
(20) Tsuda, T.; Kurihara, T.; Hoshino, Y.; Kiyama, T.; Okazaki, K.; Torimoto, T.; Kuwabata, S. *Electrochemistry* **2009**, *77*, 693.
(21) Li, C.; Zhang, D.; Han, S.; Liu, X.; Tang, T.; Zhou, C. *Adv. Mater.* **2003**, *15*, 143.
(22) Dimitrijevic, N.; Rajh, T.; Ahrenkiel, S.; Nedeljkovic, J.; Micic, O.; Nozik, A. *J. Phys. Chem. B* **2005**, *109*, 18243.
(23) Dayeh, S.; Yu, E.; Wang, D. *small* **2007**, *3*, 1683.
(24) Hammarberg, E.; Feldmann, C. *Chem. Mater.* **2009**, *21*, 771.
(25) Soulantica, K.; Maisonnat, A.; Fromen, M.; Casanove, M.; Lecante, P.; Chaudret, B. *Angew. Chem., Int. Ed.* **2001**, *40*, 448.
(26) Ganeev, R.; Ryasnyanskiy, A.; Chakravarty, U.; Naik, P.; Srivastava, H.; Tiwari, M.; Gupta, P., S *Appl. Phys. B: Laser Opt.* **2007**, *86*, 337.
(27) Chen, Q.; Tanaka, M.; Furuya, K. *Surf. Sci.* **1999**, *440*, 398.
(28) Zhao, Y.; Zhang, Z.; Dang, H. *J. Phys. Chem. B* **2003**, *107*, 7574.
(29) Du, N.; Zhang, H.; Chen, B.; Ma, X.; Liu, Z.; Wu, J.; Yang, D. *Adv. Mater.* **2007**, *19*, 1641.
(30) van de Lagemaat, J.; Barnes, T.; Rumbles, G.; Shaheen, S.; Coutts, T.; Weeks, C.; Levitsky, I.; Peltola, J.; Glatkowski, P. *Appl. Phys. Lett.* **2006**, *88*, 233503.
(31) Minami, T.; Takata, S.; Kakumu, T. *J. Vac. Sci. Technol., A* **1996**, *14*, 1689.
(32) Li, B.; Xie, Y.; Jing, M.; Rong, G.; Tang, Y.; Zhang, G. *Langmuir* **2006**, *22*, 9380.
(33) Joint Committee on Powder Diffraction Standards (JCPDS). *Powder Diffraction File 5−642*; International Center for Diffraction Data: Swarthmore, PA, 1992.
(34) Joint Committee on Powder Diffraction Standards (JCPDS). *Powder Diffraction File 6−416*; International Center for Diffraction Data: Swarthmore, PA, 1992.
(35) Nair, P.; Radhakrishnan, T.; Revaprasadu, N.; Kolawole, G.; O'Brien, P. *J. Mater. Chem.* **2002**, *12*, 2722.

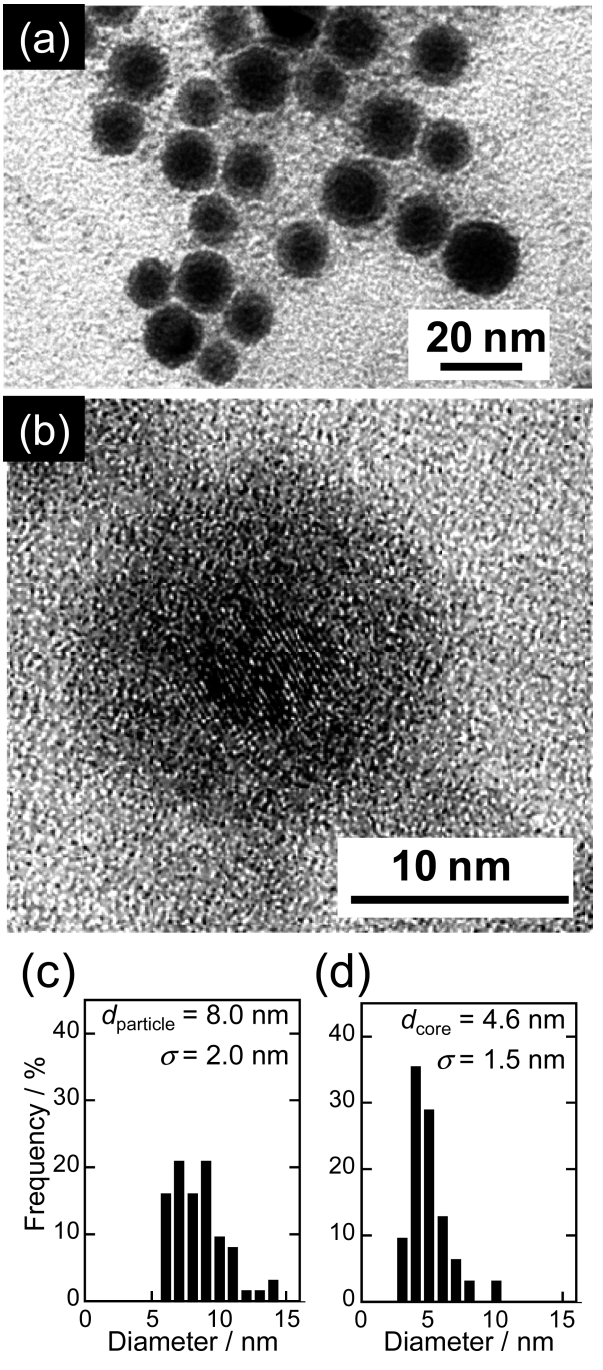

Figure 1. (a) Typical TEM image of nanoparticles prepared by In sputter deposition in EMI-BF_4. (b) High-magnification image of a nanoparticle in image a. (c) Size distribution of whole particles having an In/In_2O_3 core/shell structure, and (d) that of In cores inside the particles obtained from TEM images.

from the crystallite size estimated from XRD. These facts suggested that the surface of In metal particles was covered with an amorphous layer as supported by the following TEM measurements.

Figure 1a shows a typical TEM image of the particles obtained by In sputter deposition in EMI-BF_4. Spherical nanoparticles were observed without the formation of aggregated secondary particles. It was clearly recognized that individual particles had a core/shell structure, with the core showing a darker image than the surface shell layer. Furthermore, even when the sample stage of the

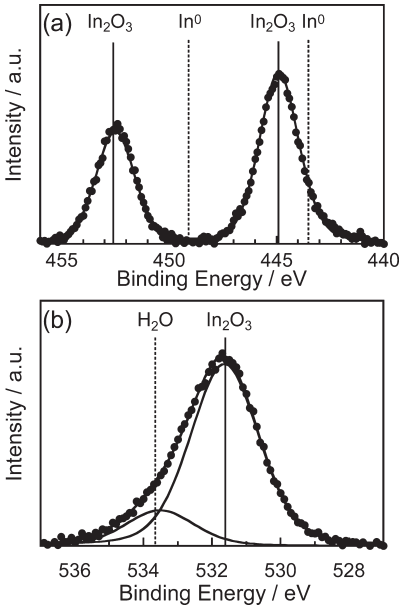

Figure 2. XPS spectra for In (a) 3d doublets and (b) O 1s of the core/shell nanoparticles.

TEM was tilted at angles from −30 to +30°, a similar core/shell structure was seen in TEM images for each particle (see Figure S3 in the Supporting Information); that is, the dark image was located at the center of the nanoparticles, indicating that the core was located almost at the center of the particle and then the shell having a uniform thickness covered the core surface. Figure 1b shows an HRTEM image of the core/shell nanoparticles. The core of darker image in a particle exhibited clear lattice fringes without exhibiting lattice mismatch or lattice defects inside the core. The interplanar spacing of lattice fringes was calculated to be 0.27 nm, which was assigned to the (101) plane of indium metal,[36] indicating that the core was a single crystal made of In metal and was covered with an amorphous shell layer.

Figure 2 shows XPS spectra of the core/shell nanoparticles shown in Figure 1a in the range of binding energies corresponding to the signals of In 3d and O 1s. Signals assigned to In $3d_{5/2}$ and In $3d_{3/2}$ were observed at 444.8 and 452.5 eV, respectively.[37] These peaks were shifted toward higher energy from the binding energies of the indium metal (In^0) but agreed with those of In_2O_3. In addition, the peaks originating from O 1s were composed of two spectral bands at 533.5 and 531.6 eV. The signal at 531.6 eV could be attributed to the lattice oxygen in In_2O_3 and that at 533.5 eV was assignable to H_2O probably adsorbed on the particle surface.[38,39] Because XPS spectra were sensitive for the surface of the particles, these results indicated that the particles as-sputter-deposited had a surface composed of indium(III) oxide. Consequently, on the basis of the results of XRD, XPS, and

(36) Lei, Y.; Chim, W. *J. Am. Chem. Soc.* **2005**, *127*, 1487.
(37) Balamurugan, B.; Kruis, F.; Shivaprasad, S.; Dmitrieva, O.; Zahres, H. *Appl. Phys. Lett.* **2005**, *86*, 083102.
(38) Faur, M.; Faur, M.; Jayne, D. T.; Goradia, M.; Goradia, C. *Surf. Interface Anal.* **1990**, *15*, 641.
(39) Nefedov, V. I.; Gati, D.; Dzhurinskii, B. F.; Sergushin, N. P.; Salyn, Y. V. *Zh. Neorg. Khim.* **1975**, *20*, 2307.

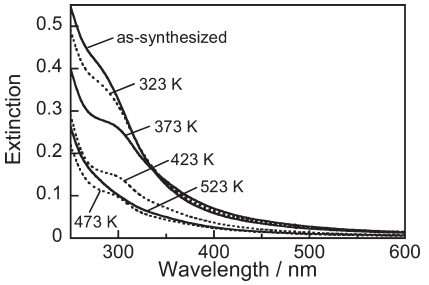

Figure 3. Changes in extinction spectra of In-sputter-deposited EMI-BF_4 solution with heat treatment in air at various temperatures. The temperatures are indicated in the figure.

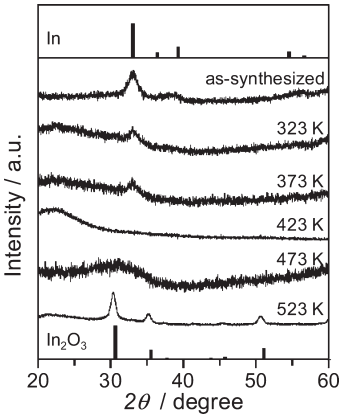

Figure 4. XRD patterns of the nanoparticles shown in Figure 3. The temperatures are indicated in the figure.

TEM observations, we could concluded that In sputter deposition in EMI-BF_4 produced core/shell-structured particles composed of a single-crystalline In metal core and amorphous In_2O_3 shell layer.

The size distribution of particles was determined by TEM measurements as shown in Figure 1a (more than 100 particles). Figure 1c and 1d show the size distribution of whole particles having a core/shell structure and that of In cores in the particles. The average size of the whole particles ($d_{particle}$) was determined to be 8.0 nm with standard deviation (σ) of 2.0 nm, which was comparable to the size determined by DLS measurement (8.1 nm), indicating that nanoparticles were highly dispersed in ILs without large aggregation. The cores of In metal had an average size (d_{core}) of 4.6 nm (σ of 1.5 nm), which was in good agreement with the size estimated from the XRD peak (4.8 nm). The shell thickness could be estimated to be 1.7 nm assuming that it was half the difference between $d_{particle}$ and d_{core}.

The expected mechanism for the formation of In/In_2O_3 core/shell nanoparticles is partial oxidation of In metal particles with O_2 contained in argon gas as an impurity or in air. Bombardment of the In foil surface with energetic argon ions caused physical ejection of surface atoms or small clusters, which were injected in ILs. This situation could make a high concentration of In species on the surface of ILs to coalesce with each other, resulting in the production of nanometer-sized In particles. Because In metal has a sufficient redox potential to be oxidized with

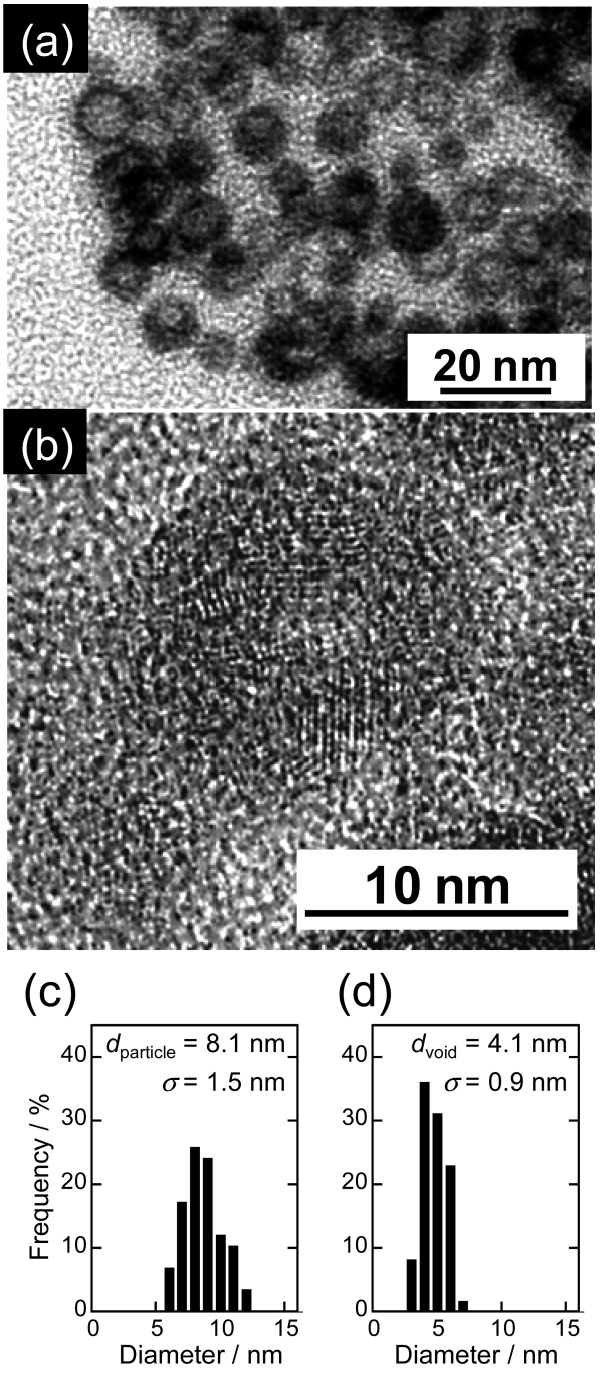

Figure 5. (a) Typical TEM image of nanoparticles in EMI-BF_4 obtained after heat treatment at 523 K in air. (b) High-magnification image of a hollow nanoparticle in image a. (c) Size distribution of In_2O_3 hollow nanoparticles and (d) that of their void spaces obtained from TEM images.

O_2 and the surface energy of nanoparticles is generally high, the surface of In nanoparticles was rapidly oxidized to form an In_2O_3 shell layer by exposure of the IL solution to air after the sputter deposition. The density of the In_2O_3 shell seems to be sufficient to prevent further oxidation of the In metal core, resulting in the formation of stable In/In_2O_3 core/shell particles.

Preparation of Hollow In_2O_3 Nanoparticles via Heat Treatment in Air. The thus-obtained EMI-BF_4 solution containing In/In_2O_3 core/shell nanoparticles was heated at various temperatures for 60 min in air. Figure 3 shows

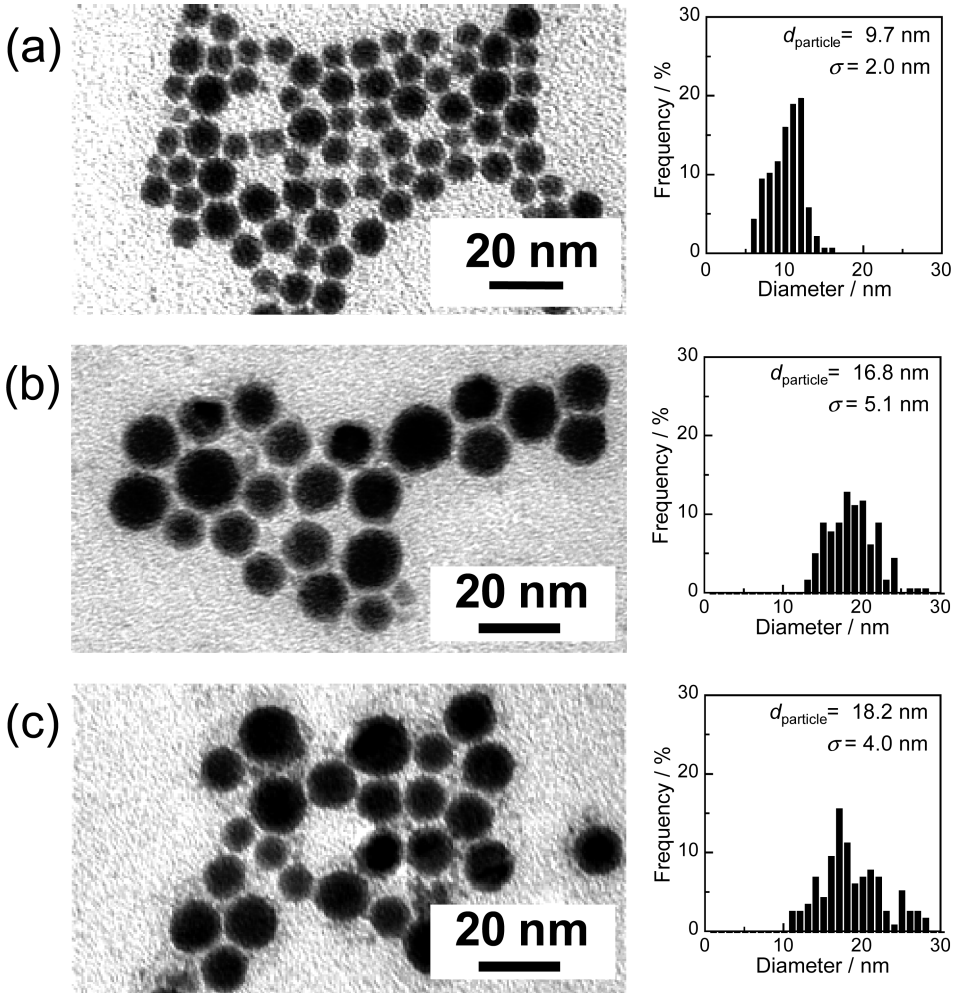

Figure 6. Typical TEM images of In/In_2O_3 core/shell nanoparticles prepared by In sputter deposition in BMI-BF_4 (a), AEI-BF_4 (b), and AMI-BF_4 (c). The size distributions of the particles are also shown beside the corresponding images.

the changes in extinction spectra of the In-deposited EMI-BF_4 solution with increase in heat treatment temperature. An absorption shoulder appeared at 280 nm for In/In_2O_3 core/shell nanoparticles, which was assigned to the surface plasmon resonance (SPR) peak of In nanoparticles.[26,28,40] The intensity of the peak at 280 nm was diminished with an increase in temperature and then completely disappeared with heat treatment at 523 K, indicating that degradation of the In metal core occurred with heat treatment. This was supported by the results of XRD analyses.

Figure 4 shows XRD patterns of the nanoparticles heat-treated at various temperatures. The crystal phase of In metal was detected for samples treated at temperatures below 373 K, but the intensity of the XRD peaks was lessened with an increase in heating temperature, the behavior being accordance with the results observed in the extinction spectra. Heat treatment at temperatures higher than 423 K caused disappearance of the peaks originating from the In metal, whereas broad diffraction peaks assigned to the (222) lattice planes of In_2O_3 emerged at around 2θ = 30° by heat treatment at 473 K and then a highly crystallized In_2O_3 phase was produced at 523 K.[34] Considering that the melting point of In is 419 K,[41] these facts suggested that the In metal cores melted with heating at temperature higher than 423 K and then were easily oxidized with O_2 to form In_2O_3.

Figure 5a shows a TEM image of crystalline In_2O_3 nanoparticles obtained with heat treatment at 523 K. Although as-sputter-deposited core/shell particles completely disappeared, spherical particles with a hollow interior were formed. TEM images of the individual particles were almost unchanged when the measurements were performed by changing the tilt angle of the TEM sample holder (see Figure S4 in the Supporting Information). This fact indicated that the spherical hollow In_2O_3 particles were formed by heat treatment with the void space being located at almost the center of each particle. An HRTEM image (Figure 5b) revealed that hollow particles had a polycrystalline shell wall composed of nanoparticles having clear lattice fringes with an interplanar spacing of 0.29 nm corresponding to the (222) of cubic In_2O_3 phase.[36]

Panels c and d in Figure 5 show the size distributions of hollow particles and their void spaces determined by TEM measurements. Hollow particles had a wide size

(40) Khanna, P.; Jun, K.; Hong, K.; Baeg, J.; Chikate, R.; Das, B. *Mater. Lett.* **2005**, *59*, 1032.

(41) Zayed, M.; Hegazy, M.; Elsayed-Ali, H. *Thin Solid Films* **2004**, *449*, 254.

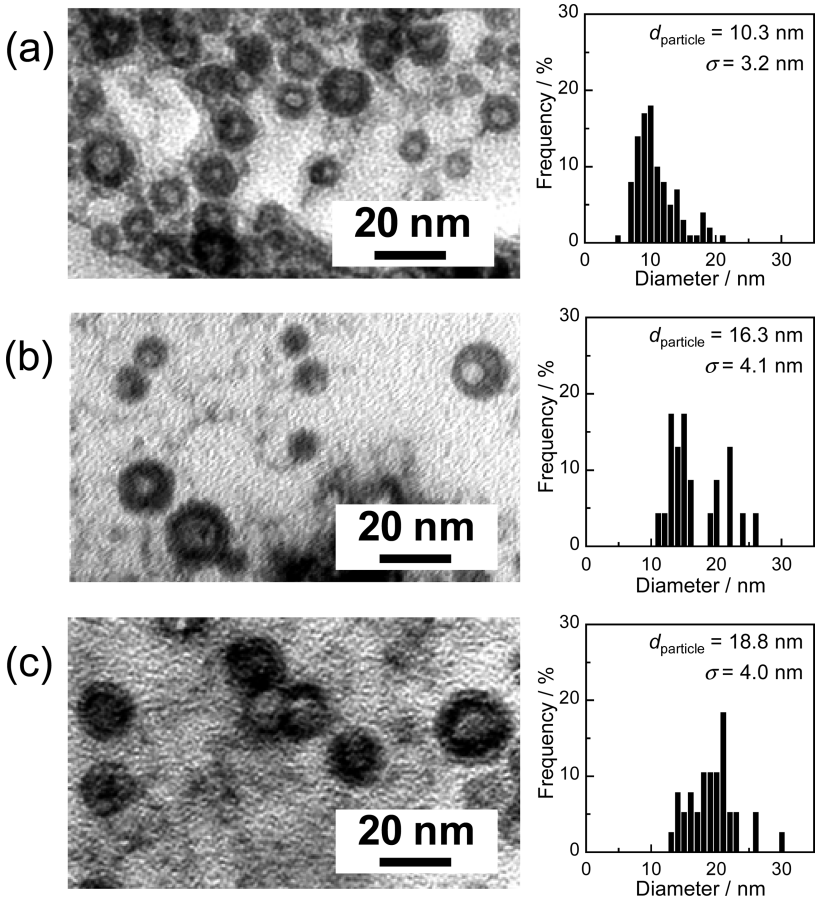

Figure 7. Typical TEM images of hollow In_2O_3 nanoparticles prepared by the heat treatment at 523 K. ILs used were (a) BMI-BF_4, (b) AEI-BF_4, and (c) AMI-BF_4. The size distributions of the particles are also shown beside the corresponding images.

distribution ranging from 6 to 13 nm, and the average diameter of whole particles ($d_{particle}$) was determined to 8.1 nm (σ of 1.5 nm), which was slightly larger than that of the In/In_2O_3 core/shell particles used as a starting material, $d_{particle}$ of 8.0 nm. In contrast, a void space smaller than the size of the In core was formed; void spaces in hollow particles with an average size (d_{void}) of 4.1 nm (σ of 0.9 nm) were formed by heating the core/shell particles with In core size of 4.6 nm. By halving the difference between $d_{particle}$ and d_{void} of hollow particles, the shell thickness could be estimated to 2.0 nm, slightly thicker than that of the shell thickness of original core/shell particles.

Size Control of the In/In_2O_3 Core/Shell Particles and the Resulting Hollow In_2O_3 Particles. It has been reported that the size of nanoparticles formed in ILs varied depending on the kind of ILs used. We therefore tried to control the size of sputter-deposited In particles by changing the kind of IL containing BF_4^- as an anionic species. TEM images of the thus-obtained particles and their size distributions are shown in Figure 6.

Sputter deposition of In produced In/In_2O_3 core/shell-structured particles in all cases, but the size of particles varied depending on the kind of IL used. Heat treatment of thus-obtained ILs at 523 K in air changed the nanostructure of particles as shown in TEM images in Figure 7. Although it was difficult to obtain clear TEM images in the case of using AMI-BF_4, it could be recognized that hollow In_2O_3 particles were produced in all kinds of ILs used, the size of which was increased with an increase in the whole size of In/In_2O_3 particles as-sputter-deposited.

Figure 8a shows average dimensions of the prepared particles: d_{core} of the In core obtained from TEM measurements is plotted as a function of $d_{particle}$ of In/In_2O_3 core/shell particles prepared in various kinds of IL. The figure also shows the dependence of d_{void} of the void space on $d_{particle}$ of the hollow In_2O_3 particles obtained after heat treatment in ILs. The size of the In metal core seems to linearly increase from 8 to 20 nm by enlargement of the whole size of In/In_2O_3 core/shell particles. Figure 8b shows the In_2O_3 shell thickness of core/shell particles estimated from the results in Figure 8a. Interestingly, the shell thickness was almost constant regardless of the size of the In core, the average thickness being ca. 1.9 nm. This fact indicated that an In_2O_3 shell with a thickness of ca. 1.9 nm could effectively prevent the penetration of O_2 through the shell layer to the In metal core surface from air and/or IL solution at room temperature.

Heat treatment of In/In_2O_3 particles at 523 K produced hollow particles with a slight increase in $d_{particle}$ (0.1−0.6 nm), except for the case of using AEI-BF_4 as an IL. The value of d_{void} linearly increased from 4 to 10 nm with an increase in $d_{particle}$ of hollow particles, indicating that the structure of thus-obtained hollow In_2O_3 nanoparticles

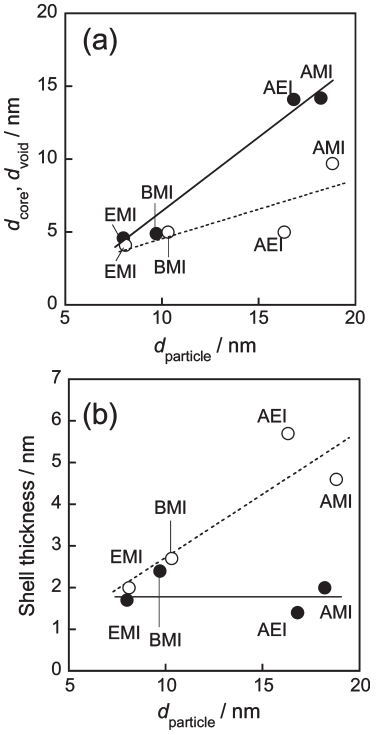

Figure 8. (a) Dependence of d_{core} (solid circles) and d_{void} (open circles) on the whole size ($d_{particle}$) of In/In_2O_3 core/shell particles and that of hollow In_2O_3 particles, respectively. (b) Relationship between shell thickness and $d_{particle}$ of In/In_2O_3 core/shell particles (solid circles) or hollow In_2O_3 particles (open circles). Cationic species of ILs used are indicated in the figure.

could also be controlled by selecting the kind of IL used for the sputter deposition of In. It should be noted that d_{void} was smaller than d_{core} of the corresponding core/shell particles (Figure 8a). Furthermore, as shown in Figure 8b, the shell thickness of hollow particles was larger than that of In/In_2O_3 particles (ca. 1.9 nm on average) and increased with an increase in $d_{particle}$ of hollow particles.

The formation of a void space by oxidation of the In metal core with O_2 is reasonably explained by the Kirkendall effect in a nanometer scale.[42,43] Though the In/In_2O_3 core/shell particles were stable at room temperature because of coverage of the In core with an oxide shell layer to prevent further oxidation of In metal, heat treatment of core/shell particles in ILs at 523 K, which is higher than the melting point of bulk In metal (419 K), accelerated the oxidation of the In metal core. If only indium ions diffused outward through the shell to form the In_2O_3 oxide layer at the outer surface of the shell, the void space would be formed inside the particle, the size being comparable to the size of the In core. As shown in Figure 8a, the size of the final void space became smaller than that of the initial In metal core, especially for larger In/In_2O_3 particles. This fact indicated that in addition to the predominant outward diffusion of In ions, an inward transport of oxygen ions occurred, and an In_2O_3 crystal could thus be grown on both the inner concave and outer convex surfaces of the oxide shell layer.

Conclusion

Sputter deposition of indium in ILs resulted in the production of stable In metal particles without additional agents, being different from conventional chemical methods using highly active agents to reduce indium ions. The thus-obtained In metal nanoparticles were covered by an amorphous In_2O_3 layer (ca.1.9 nm in thickness), that is, In/In_2O_3 core/shell particles, the core size of which was tunable from ca. 8 to 20 nm depending on the kind of IL used. Heat treatment of thus-obtained particles at 523 K in air removed the In metal core, resulting in the formation of hollow particles made of crystalline In_2O_3, the void space of which could be enlarged from 4 to 10 nm by increasing the size of core/shell particles used as the starting material. The sizes of both In/In_2O_3 core/shell particles and hollow In_2O_3 particles were controlled by selecting an appropriate kind of IL. Because In metal particles are useful as a starting material to convert them to In-based compound materials, such as InP quantum dots,[44] the size tunability of In particles obtained by the present strategy will enable precise control of the nanostructure of the resulting target materials. On the other hand, In_2O_3 is well-known as an n-type semiconducting oxide having a band gap of around 3.6 eV. Precise control of the hollow structure of In_2O_3 nanoparticles should lead to the development of novel photocatalysts for molecular-size-selective reactions and for solar cells, in which the void space can act as a nanoflask for reaction sites and/or molecular adsorption sites. A study along this line is currently in progress.

Acknowledgment. This work was supported by a Grant-in-Aid for Scientific Research (A) (20245031) from the Japan Society for the Promotion of Science and by a Grant-in-Aid for Scientific Research on Priority Areas "Strong Photons-Molecules Coupling Fields (No. 470)" (No. 19049009) and "Science of Ionic Liquids (No. 452)" (20031012) from the Ministry of Education, Culture, Sports, Science and Technology of Japan. T.S. expresses his appreciation to The Global COE (Center Of Excellence) Program "Elucidation and Design of Materials and Molecular Functions" of Nagoya University.

Supporting Information Available: Additional images (PDF). This material is available free of charge via the Internet at http://pubs.acs.org.

(42) Yin, Y.; Rioux, R.; Erdonmez, C.; Hughes, S.; Somorjai, G.; Alivisatos, A. *Science* **2004**, *304*, 711.
(43) Fan, H.; Gosele, U.; Zacharias, M. *Small* **2007**, *3*, 1660.
(44) Nedeljkovic, J.; Micic, O.; Ahrenkiel, S.; Miedaner, A.; Nozik, A. *J. Am. Chem. Soc.* **2004**, *126*, 2632.